---

**Article:**
Criado, M. and Provis, J.L. orcid.org/0000-0003-3372-8922 (2018) Alkali activated slag mortars provide high resistance to chloride-induced corrosion of steel. Frontiers in Materials, 5. 34. ISSN 2296-8016

https://doi.org/10.3389/fmats.2018.00034

---

frontiers in Materials

ORIGINAL RESEARCH
published: 04 June 2018
doi: 10.3389/fmats.2018.00034

# Alkali Activated Slag Mortars Provide High Resistance to Chloride-Induced Corrosion of Steel

*Maria Criado and John L. Provis**

*Department of Materials Science and Engineering, The University of Sheffield, Sheffield, United Kingdom*

The pore solutions of alkali-activated slag cements and Portland-based cements are very different in terms of their chemical and redox characteristics, particularly due to the high alkalinity and high sulfide content of alkali-activated slag cement. Therefore, differences in corrosion mechanisms of steel elements embedded in these cements could be expected, with important implications for the durability of reinforced concrete elements. This study assesses the corrosion behavior of steel embedded in alkali-activated blast furnace slag (BFS) mortars exposed to alkaline solution, alkaline chloride-rich solution, water, and standard laboratory conditions, using electrochemical techniques. White Portland cement (WPC) mortars and blended cement mortars (WPC and BFS) were also tested for comparative purposes. The steel elements embedded in immersed alkali-activated slag mortars presented very negative redox potentials and high apparent corrosion current values; the presence of sulfide reduced the redox potential, and the oxidation of the reduced sulfur-containing species within the cement itself gave an electrochemical signal that classical electrochemical tests for reinforced concrete durability would interpret as being due to steel corrosion processes. However, the actual observed resistance to chloride-induced corrosion was very high, as measured by extraction and characterization of the steel at the end of a 9-month exposure period, whereas the steel embedded in WPC mortars was significantly damaged under the same conditions.

**Keywords: alkali-activated cement, blast furnace slag, white Portland cement, corrosion, chloride, sulfide**

OPEN ACCESS

***Edited by:***
*Andrew C. Heath,*
*University of Bath, United Kingdom*

***Reviewed by:***
*Kostas A. Komnitsas,*
*Technical University of Crete, Greece*
*Ru Mu,*
*Hebei University of Technology, China*

***Correspondence:**
*John L. Provis*
*j.provis@sheffield.ac.uk*

***Specialty section:***
*This article was submitted to Structural Materials, a section of the journal Frontiers in Materials*

***Received:*** *30 March 2018*
***Accepted:*** *17 May 2018*
***Published:*** *04 June 2018*

***Citation:***
*Criado M and Provis JL (2018) Alkali Activated Slag Mortars Provide High Resistance to Chloride-Induced Corrosion of Steel. Front. Mater. 5:34. doi: 10.3389/fmats.2018.00034*

## INTRODUCTION

Steel reinforcing elements (rebars) embedded in Portland cement (PC)-based concretes are protected from corrosion by a thin oxide film that is formed and maintained on rebar surfaces due to the high pH of the surrounding concrete (Böhni, 2005). However, it is now becoming evident that the nature and stability of this oxide film change when the surrounding concrete is produced with non-Portland cements such as alkali-activated materials (AAMs) (Mundra et al., 2017a,d; Criado et al., 2018), and this is expected to be important when considering such materials for use in infrastructure applications involving chloride exposure. During the hydration of PC, portlandite [$Ca(OH)_2$] forms as an important hydration product, and plays important role in delaying the onset of the corrosion of embedded steel, as it can maintain the high pH of the cement pore solution through a buffering mechanism (Bertolini et al., 2013). However, in AAMs portlandite is not typically identified as a reaction product (Lloyd et al., 2010), and therefore, the availability

(or conversely, leaching) of $OH^-$ ions from the pore solution at the steel-concrete interface will have a greater influence in ensuring the stability of this protective layer in AAMs (Mundra et al., 2017d).

Various studies have demonstrated that a mixture of blast furnace slag (BFS) (even up to 70%) blended with Portland cement affected the corrosion process of steel rebar; the presence of BFS improved the corrosion resistance by slowing down chloride ingress, and decreased the corrosion rate and delayed the time at which corrosion occurs (Huang et al., 1996; Gu et al., 2000; Cheng et al., 2005; Yeau and Kim, 2005; Song and Saraswathy, 2006; Topçu and Boga, 2010; Garcia et al., 2014). This advantageous formation of a dense, impermeable microstructure through generation of additional calcium silicate hydrate (C-S-H)-type reaction products is particularly evident at higher BFS content and after a longer period of curing (Yeau and Kim, 2005; Topçu and Boga, 2010). Slag-blended Portland cements, and alkali-activated slag cements, also generate hydrotalcite-group phases as a hydration product, and this provides chemical binding effects (Ke et al., 2017a,b) that can further restrict the ingress of chloride.

However, fewer studies have been published regarding the actual corrosion process of steel embedded in alkali activated slag mortars in the presence of chloride (Holloway and Sykes, 2005; Torres Gomez et al., 2010; Park et al., 2015; Ma et al., 2016). AAS mortars activated with $Ca(OH)_2$ presented a higher corrosion resistance than AAS mortars activated with KOH and NaOH activators, which was attributed to the formation of $Ca(OCl)_2$ to remove free chloride from the pore solution, and thus to mitigate the corrosion risk (Park et al., 2015). Ma et al. (2016) found that an increased alkali concentration in the activator, and the use of a sodium silicate activator with a modulus (molar ratio $SiO_2/Na_2O$) of 1.5, gave a desirable microstructure which improved the resistance to chloride transport and corrosion. Moreover, the corrosion rate of the steel bars was significantly influenced by the free sulfide concentration in these alkaline concretes, consistent with a recent classification proposed by Mundra et al. (2017b).

The presence of sulfide in the pore solution of concrete can significantly reduce its redox potential, which in classical concrete electrochemistry is considered to indicate steel depassivation. However, chemical reactions at the steel-concrete interface which involve sulfide have recently been observed to protect the embedded steel from corrosion to a certain extent (Criado et al., 2018). Moreover, the onset of chloride-induced pitting on the steel surface in simulated alkali-activated slag pore solution depends on both the concentration of sulfide and the time of exposure, due to the alteration of passive film chemistry in the presence of a strong reductant, which is beneficial in restricting corrosion if the sulfide concentration is sufficiently high (Mundra et al., 2017b). Conversely, Tromans (1980) observed that sulfide could be incorporated into magnetite, reducing the potential domain where the passive film is stable, and in that study an increase in current density took place, which was interpreted as indicating that the protective properties of the passive layer were decreased. Therefore, the presence of sulfide in BFS-containing cements means that the redox potential of their pore solutions will be much lower than that measured in PC, and consequently the corrosion behavior of the steel in AAS will be different from that which is observed in PC. However, much remains unknown about the details and mechanisms of this process.

The core aim of this study is to evaluate the corrosion behavior of steel embedded in sodium silicate-activated BFS mortars exposed to four different environments: an alkaline solution representing pore solution chemistry to prevent leaching (as a reference case), an alkaline chloride-rich solution to induce chloride transport without alkali leaching, plain water, and standard laboratory conditions (open to atmosphere). The corrosion behavior is assessed using electrochemical techniques, as well as by extraction and analysis of the steel rebars after a 9-month exposure period. White Portland cement (WPC) mortars and blended cement mortars (50 wt% WPC and 50 wt% BFS) are also tested for comparative purposes.

# EXPERIMENTAL METHODOLOGY

## Materials and Environments

Corrugated mild steel rebars ($\phi = 12$ mm) conforming to BS 4449:2005 + A3:2016 (British Standards Institute, 2016) were obtained from a local supplier in Sheffield, UK. Their chemical composition (mass %) is 0.21 C, 0.23 Si, 0.76 Mn, 0.04 P, 0.03 S, 0.13 Cr, 0.20 Ni, 0.47 Cu, 0.02 Mo, and balance Fe. Rebars were cut using an abrasive disc to produce both 100 mm-long test specimens. Prior to electrochemical testing, the reinforcement bars with an intact as-received rust layer were embedded in mortars, with ends masked with an epoxy resin (Sikagard-62) coating to leave an exposed surface area of 10 $cm^2$.

To produce the mortar blocks in which the rebars were embedded, a ground granulated BFS supplied by Ecocem, and a WPC (Lafarge Blue Circle Snowcrete, classified as CEM I 52.5R under BS EN 197-1; European Committee for Standardization, 2011) were used. Their oxide compositions, determined by X-ray fluorescence (XRF), are shown in **Table 1**.

The activator used in alkali-activated slag mortars was prepared by fully dissolving anhydrous sodium metasilicate powder (Sigma-Aldrich, $Na_2SiO_3$) into distilled water, and allowing the solution to cool to room temperature. BFS was then activated by mixing this powder with a solution containing 7 g sodium metasilicate per 100 g BFS, at a water to total solids (slag + $Na_2SiO_3$) mass ratio of 0.40. The WPC and the blended cement (50:50 BFS:WPC, denoted WPS) were hydrated at a water to binder mass ratio of 0.45, as the water/cement ratio needed to be increased to give sufficient flow to allow casting of specimens.

Prismatic mortar specimens were prepared with dimensions of 80 × 50 × 50 mm, each containing two mild steel bars with a diameter of 12 mm and length of 100 mm, **Figure 1A** (Criado et al., 2018). The rebars were positioned with a low cover depth, 4.5 mm, to minimize the effect of the time taken for chloride to diffuse to the steel surface, as the focus of this study is the corrosion process rather than chloride transport. A CEN standard sand (European Committee for Standardization, 2005) was used to prepare mortars, at a

**TABLE 1 |** Chemical composition of the raw materials used, obtained by XRF.

| Oxide (wt.%) | CaO | $SiO_2$ | $Al_2O_3$ | MgO | $SO_3$ | $Fe_2O_3$ | $TiO_2$ | MnO | $K_2O$ | Other | LOI |
|---|---|---|---|---|---|---|---|---|---|---|---|
| BFS | 41.8 | 36.0 | 11.3 | 6.5 | 0.7* | 0.3* | 0.5 | 0.3 | 0.4 | 0.2 | 2.0 |
| WPC | 66.5 | 23.7 | 3.9 | 0.9 | 2.6 | 0.2 | – | – | 0.5 | 1.2 | 1.2 |

*LOI is the loss on ignition at 1,000°C. *S and Fe are present at least in part in reduced forms in the BFS, but are represented as oxides in the XRF analysis.*

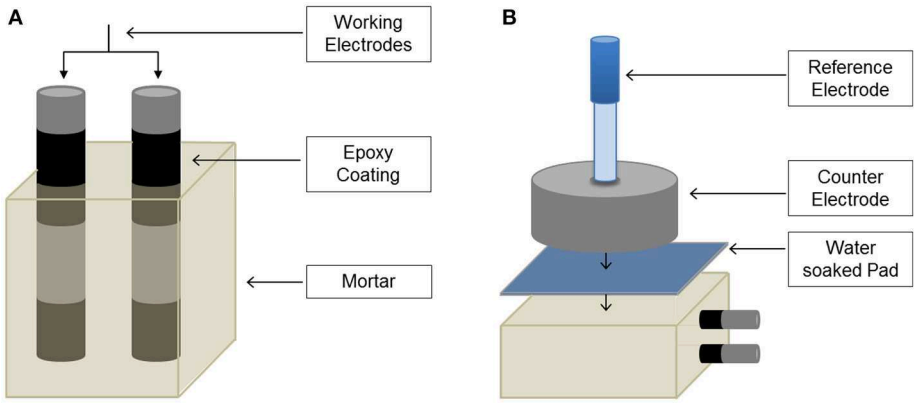


**FIGURE 1 | (A)** Reinforced prismatic sample geometry, and **(B)** electrochemical testing setup (Criado et al., 2018).

sand/binder mass ratio of 3.0. Mortars were mechanically mixed using a Hobart mixer, cast into steel molds with clamps to correctly position the rebars, and sealed to enable the mortars to harden at room temperature without drying. After 24 h the specimens were demolded, wrapped with cling film, and cured at 20 ± 2°C for 7 days, and then fully immersed in the selected environments to initiate the exposure period. BFS mortars were immersed in either 1 M NaOH (Sigma Aldrich) solution with and without the addition of 3.5% NaCl (EMD Chemicals), or in water. WPS and WPC mortars were immersed in 0.027 M $Ca(OH)_2$ (Alfa Aesar) solution with and without 3.5% NaCl, or in water. The different NaOH or $Ca(OH)_2$ solutions were designed to prevent leaching of sodium from the BFS samples and calcium from the WPS and WPC samples (in contrast to the water immersion), and were not replaced during the test period. The pH of each immersion solution was measured regularly using an Oakton Acorn series pH meter. Duplicate mortar specimens were made for each mortar/steel system, giving four test bars for each condition. Two additional specimens of each type of mortar were exposed to standard laboratory conditions (open storage at ambient temperature of 21 ± 5°C and 50 ± 20% relative humidity).

# Methods

## Electrochemical Testing

Corrosion potential ($E_{corr}$), linear polarization resistance (LPR) and electrochemical impedance spectroscopy (EIS) measurements were recorded periodically up to 180 days of immersion in the different environments. A conventional three-electrode cell was used for electrochemical measurements, **Figure 1B**. The steel bars embedded in the prismatic mortar specimens acted as working electrode and a stainless steel cylinder (acting as counter electrode) was placed above the mortar. The counter electrode had the same size as the mortars, achieving a uniform distribution of current lines, and a centrally drilled hole where an Ag/AgCl (filled with 3 M KCl) electrode was positioned to act as the reference electrode. A pad soaked in tap water was used to facilitate the electrical measurements.

A Princeton Applied Research VersaSTAT 3F was utilized for the electrochemical measurements. LPR was determined by applying $\Delta E$ of ±10 mV vs. $E_{corr}$, at a scan rate of 0.1667 mV $s^{-1}$. EIS measurements were recorded at $E_{corr}$ with a 10 mV root mean square (rms) amplitude excitation voltage, in a frequency range from 1 MHz to 1.58 mHz, with a logarithmic sweeping frequency of 5 points per decade. LPR and EIS measurements were performed after the $E_{corr}$ was stabilized for at least 30 min. The corrosion current density ($i_{corr}$) was calculated using the Stern-Geary equation (Stern and Geary, 1957): $i_{corr} = B/R_p$, adopting $B$-values of 52 or 26 mV for carbon steel in the passive or active (corroding) state, respectively (Andrade et al., 1986). These values of $B$ could show some divergences when steel is embedded in AAMs; for example, Babaee and Castel (2016) observed that the $B$-values obtained from polarization curves in alkali-activated blended (fly ash and BFS) concretes were $13 < B < 20$ for passive samples and $45 < B < 58$ for active samples. Therefore, the utilization of conventional $B$-values determined in Portland cement-based materials could lead to uncertainty in determination of the $i_{corr}$ of alkali-activated corroding systems. However, more experimental results are necessary to confirm this, particularly considering

the complexity of the redox chemistry of sulfur supplied by BFS.

### Corrosion Product Analysis

The nature of the corrosion products formed on the steel surface was evaluated through Raman spectroscopy, using a Renishaw InVia Raman Microscope equipped with a 514.5 nm laser and a Leica microscope. The spectra were obtained with 50× magnification objective lenses. The laser power was 1 mW, the integration time was 15 s, and 3 accumulations were collected. The Raman shift was calibrated before measurements according to the silicon peak at 520 $cm^{-1}$. The software employed for data acquisition and analysis was WIRE 3.4.

## RESULTS AND DISCUSSION

**Figure 2** shows the $E_{corr}$ values of steel rebars embedded in the three mortars: BFS, slag, and WPC mixture (WPS) and white cement Portland (WPC), under the different exposure environments as a function of time. According to ASTM C876-15 (ASTM International, 2015), for an Ag/AgCl (filled with 3 M KCl) reference electrode, the corrosion state of rebar can be assessed as follows: $E_{corr} > -310$ mV indicates a 90% chance of having no corrosion, while $E_{corr} < -460$ mV indicates a 90% probability of having corrosion. However, the presence of sulfide anions supplied by the BFS can significantly reduce the redox potential of the pore solution around the rebar, meaning that the cathode is not able to generate a current that overcomes the $HS^-$ oxidation peak. Thus, it is possible that these established criteria used for Portland cement may not be valid for cements that are very rich in slag; this possibility will be examined in detail throughout this paper.

In the alkaline solution, **Figure 2A**, the BFS specimens only showed $E_{corr}$ values less negative than −310 mV during the first 2 days of immersion. After that time, $E_{corr}$ shifted rapidly to more negative values ($< -460$ mV), which would usually be taken to indicate a high risk of corrosion (ASTM International, 2015). However, this is clearly not an indication of chloride-induced corrosion, which could not occur since the immersion solution did not contain any chloride. Glasser has previously observed that in blended slag-rich mortars, slag dissolution releases sulfide ions into the pore solution, leading to a significant reduction in redox potential (Glasser, 1991, 2001). The specimens were totally immersed in the alkaline medium, and no oxygen entered into the specimen, and this led to strongly reducing conditions where sulfide was the dominant redox-active species. Moreover, any available oxygen can be consumed locally by the sulfide species becoming oxidized, either in part or in full (Holloway and Sykes, 2005; Ma et al., 2016). In those aqueous systems, where aqueous sulfide is in excess over $Fe^{3+}$, iron is partially reduced and the $Fe^{2+}$ generated can react with $S^{2-}$ to precipitate as FeS (Wan et al., 2017). In this system, considering the pre-oxidized nature of the rebar surface embedded into the mortar specimens, it is highly likely that a complex iron sulfide

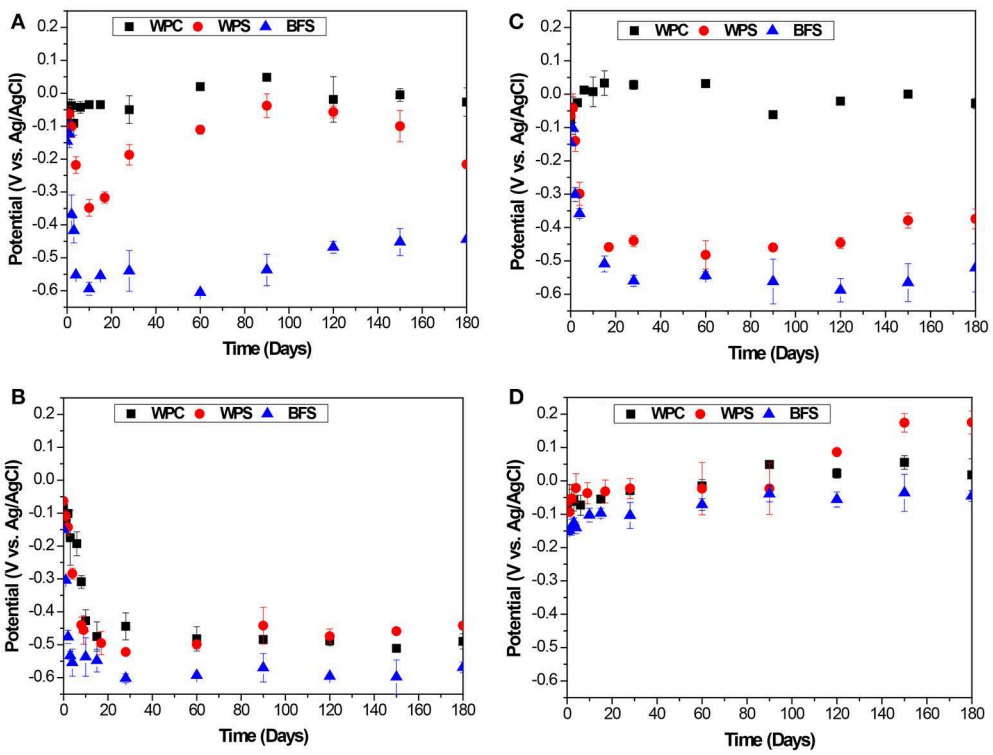


**FIGURE 2 |** Evolution of the potential values as a function of time, for steel embedded in BFS, WPS, and WPC mortars immersed in **(A)** alkaline solution, **(B)** alkaline chloride-rich solution, **(C)** water, and exposed to **(D)** standard laboratory conditions, with 7 days of curing prior to immersion or exposure.

layer is formed on the steel surface at such negative potentials (Criado et al., 2018). The absence of oxygen at the surface of the rebar inhibits the cathodic reaction, and so corrosion is controlled.

For WPS specimens in $Ca(OH)_2$ solution, the $E_{corr}$ values were generally about −0.200 V vs. Ag/AgCl or more noble, although a brief dip below this was observed in the first days of immersion. These values of potential were close to those obtained for steel rebars embedded in WPC mortars, which remained fairly constant or attained nobler values throughout the entire duration of exposure. Both WPS and WPC immersed in $Ca(OH)_2$ solutions retained $E_{corr}$ values more positive than −310 mV, showing that the steel was in a passive state, as would be expected for these cements in a chloride-free environment. After 120 days of immersion, the $E_{corr}$ values of WPS mortars do show some reduction, which could be because the reaction of BFS is the main ongoing hydration process at this time, releasing sulfide ions.

In the alkaline chloride-rich solution, **Figure 2B**, the $E_{corr}$ values of the BFS specimens decreased to a very similar level to the alkaline chloride-free exposure environment, reaching values of −0.450 V vs. Ag/AgCl or more active after 4 days. Similar levels were also reached after 9 days for WPS mortars and after 15 days for WPC mortars. According to ASTM C876-15 (ASTM International, 2015), these values of potential indicate a high probability of corrosion. The initiation of corrosion of the steel rebar embedded in WPC mortar is identified to be a consequence of the breakdown of the passive film induced by the chloride ions. In BFS mortars, a decrease in steel potential could also correspond to the presence of sulfide in the pore solution as described above and previously (Criado et al., 2018); the situation for the WPS mortars requires further analysis as this blended system could potentially be following one or the other of these extreme cases, but the fact that immersion in a chloride-free $Ca(OH)_2$ solution did not lead to a lasting drop in potential, unlike the chloride-rich case, indicates that some corrosion is in fact likely to be taking place. It is notable that the $E_{corr}$ values determined here for BFS samples are ∼100 mV more negative than those which were presented previously (Criado et al., 2018) for samples of longer curing duration (28 days, cf. 7 days here), indicating that the ongoing reaction of slag grains during curing is also important in defining the redox environment inside the cements.

For samples immersed in water, **Figure 2C**, the steel embedded in BFS and WPC specimens exhibited the same behavior as in the alkaline chloride-free solutions. For WPS specimens, a potential drop occurred after 28 days of immersion in water and $E_{corr}$ stabilized between −0.450 and −0.380 V vs. Ag/AgCl. It appears that there is some interaction between the leaching of dissolved species (potentially calcium) from the pore solution and the changes in potential due to the release of sulfide from the slag, but there is not an immediately evident explanation for the observed behavior. In standard laboratory conditions, **Figure 2D**, all specimens showed $E_{corr}$ values more positive than −0.152 V vs. Ag/AgCl, where the steel is not considered to be at risk of corrosion.

**Figure 3** shows a photograph of the surface of the original steel, which had some regions of reddish stains distributed randomly, indicating the presence of a rust layer. Raman spectra of these stains showed peaks attributed to lepidocrocite (γ-FeOOH): well-defined peaks at 250 (the most intense), 305, 378, 528, 653, 1,080, and 1,300 $cm^{-1}$ (Larroumet et al., 2007; L'Hostis et al., 2013). The presence of lepidocrocite as the main constituent of the rust layer formed on steel exposed to the atmosphere is common; several authors have observed that crystalline lepidocrocite is the first phase to form on the steel surface (Misawa et al., 1974; de la Fuente et al., 2016).

**Figure 4** shows the surface aspects and Raman spectra of the rebars extracted from the three types of mortar after immersion in the alkaline chloride-rich solutions. Raman spectra of iron compounds formed on the rebars in all mortars exposed to the alkaline solution, water and standard laboratory conditions after 270 days were similar and the compound identified on the surface of all rebars was lepidocrocite, corresponding to the mineralogy of the initial rust layer, but also potentially newly formed in contact with the cements.

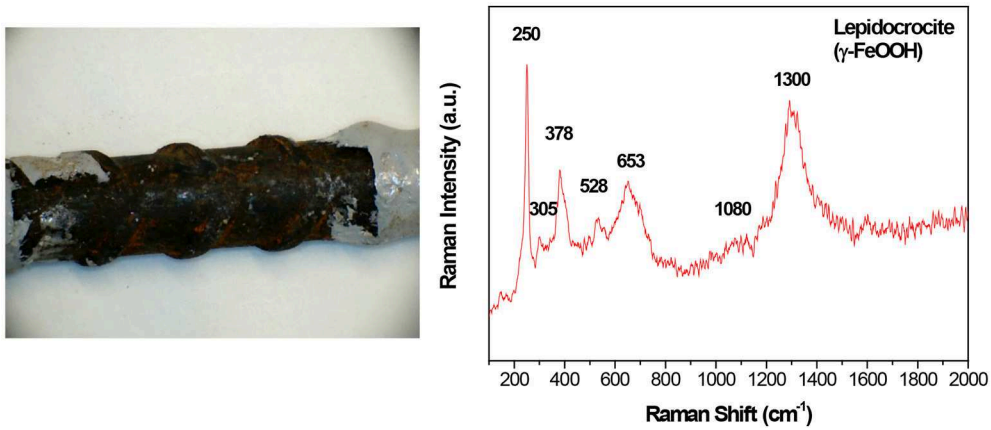


**FIGURE 3 |** Photograph of the surface of the original steel, and Raman spectrum of the rust layer detected on its surface.

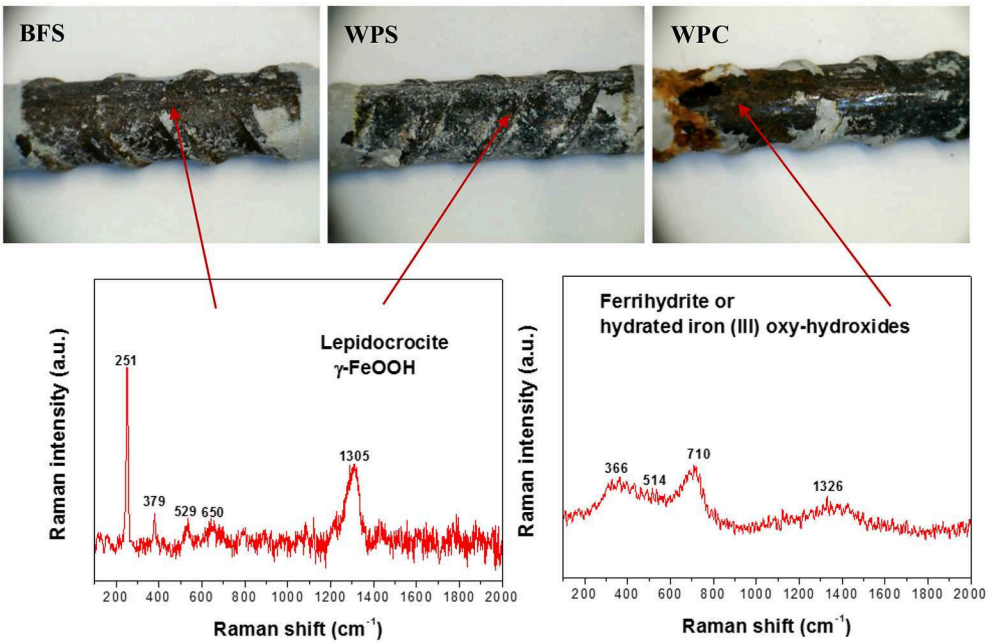


**FIGURE 4 |** Photographs and *in situ* Raman spectra of the steel rebars extracted from BFS, WPS, and WPC mortars that had been immersed in the alkaline chloride-rich solutions for 270 days.

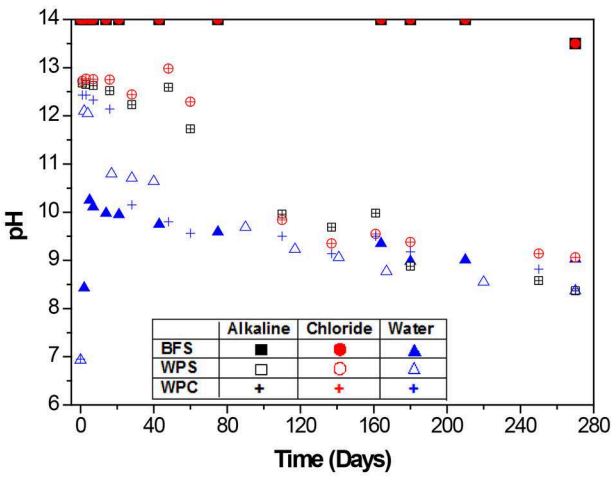


**FIGURE 5 |** Measured pH values of the three environments: alkaline and alkaline chloride-rich solutions, and water, in which BFS, WPS, and WPC mortars were immersed.

In the alkalinechloride-rich solution, new corrosion products were found on the steel embedded in WPC mortars, specifically a hydrated iron (III) oxy-hydroxide, most likely ferrihydrite, although the assignment to a particular phase is very difficult due to the low crystallinity and/or nanometric size of these compounds. The Raman spectra of ferrihydrite and other hydrated iron (III) oxy-hydroxide show a strong band around 710 $cm^{-1}$ and weaker bands around 370, 510, and 1,320 $cm^{-1}$ (Neff et al., 2006; Ghantous et al., 2017). The presence of four broad peaks in the Raman spectrum for the steel extracted from WPC mortar in **Figure 4** confirms their formation in this case. However, in the spectra of the steel bars extracted from BFS and WPS mortars, the only ordered compound detected was lepidocrocite.

Taking in account the fact that sulfide oxidation rates have been observed to be relatively high in the presence of lepidocrocite (the compound detected in the original rust layer) compared to other iron oxides (Wan et al., 2017), the formation of complex iron sulfide compounds on the steel surface was expected. However, the presence of these compounds was difficult to confirm by Raman spectroscopy, since either the main Raman peak overlaps with the peaks of lepidocrocite in the case of $Fe_7S_8$ or pyrrhotite (R060440 RRuff ID), or the structure of the phase is disordered, hindering its identification through Raman spectroscopy in the case of $Fe_{1+x}S$ ($x = 0$–$0.07$) or mackinawite (R060388 RRuff ID). The formation of iron sulfide compounds was observed through X-ray photoelectron spectroscopy when specimens of this same steel were immersed in simulated pore solution of alkali-activated slag cements (Mundra et al., 2017c), supporting the evidence presented here from real mortars.

**Figure 5** shows the evolution of pH values of the different environments in which the BFS, WPS, and WPC mortars were immersed. Measured pH values of about 13.5–14 were obtained for the 1 M NaOH and 1 M NaOH + 3.5% NaCl solutions, used for BFS mortars. The pH values measured when WPS and WPC mortars were immersed in the alkaline solution [0.027 M $Ca(OH)_2$] were identical, as were the pH values obtained when both mortars were immersed in the alkaline chloride-rich

solution (0.027 M $Ca(OH)_2$ + 3.5% NaCl); these were between 12.1 and 12.8 for the first 60 days. With time, these values decreased, reaching values of ∼8.4 in the $Ca(OH)_2$ solution and ∼9.1 in the $Ca(OH)_2$-NaCl solution after 270 days of immersion of the samples, attributed to atmospheric carbonation of the solution. For immersion in water, the pH value initially jumped due to the leaching of alkaline components from the cements, but there was then a drop of about 2 units after 15 days for WPS mortars and after 28 days for WPC mortars, with the final pH stabilizing around 8.4 in both cases. When BFS mortars were immersed in water, the pH values were lower than those obtained for the other two mortars at early age. However, this changed less over time, remaining at 9.1 at 270 days. These results do not show an obvious connection to the trends in open circuit potential as shown in **Figure 2**; it is therefore very unlikely that pH effects are controlling the electrochemistry of these specimens during testing.

**Figure 6** shows corrosion current density ($i_{corr}$) values determined for steel rebars embedded in BFS, WPS, and WPC mortars under the different environments as a function of exposure time. For binders based on Portland cement, it has been proposed that a corrosion current higher than 1 μA/cm$^2$ indicates a high risk of corrosion, whereas a corrosion current between 0.1 and 0.5 μA/cm$^2$ is a sign of low to moderate corrosion activity (Andrade and Alonso, 1996). In the mortars immersed in alkaline solution, **Figure 6A**, the $i_{corr}$ values for BFS mortars were higher than 1 μA cm$^{-2}$ after 3 days of immersion, while the WPS mortars also presented $i_{corr}$ values between 0.5 and 1 μA cm$^{-2}$ after 30 days of immersion. However, it is not possible that the rebar in these samples was already exhibiting a very high corrosion rate, as no aggressive species were introduced. Also, the $i_{corr}$ values of the rebar embedded in WPC mortars were as expected ($i_{corr}$ < 0.1 μA cm$^{-2}$), indicating the steel maintained its passivity. Corresponding trends are observed in **Figure 6C** for the samples immersed in water, while in the standard laboratory conditions, **Figure 6D**, the three types of specimen presented passivity with $i_{corr}$ values ranging between 0.05 and 0.30 μA cm$^{-2}$.

In **Figure 6B**, the electrochemical results for the slag-containing samples immersed in alkaline chloride-rich environments also appear to show corrosion, and this may superficially be attributed to the chloride present; however, **Figure 4** shows that no corrosion took place in the actual steel surfaces in either BFS or WPS, and so these measurements must also be considered to support the contention that $i_{corr}$ calculated in the conventional way is an ineffective measure of corrosion activity in slag-containing samples.

The presence of sulfide in slag-containing matrices is clearly affecting the results obtained through electrochemical measurements, as the oxidation of reduced sulfur species at the steel-mortar interface is not distinguishable in

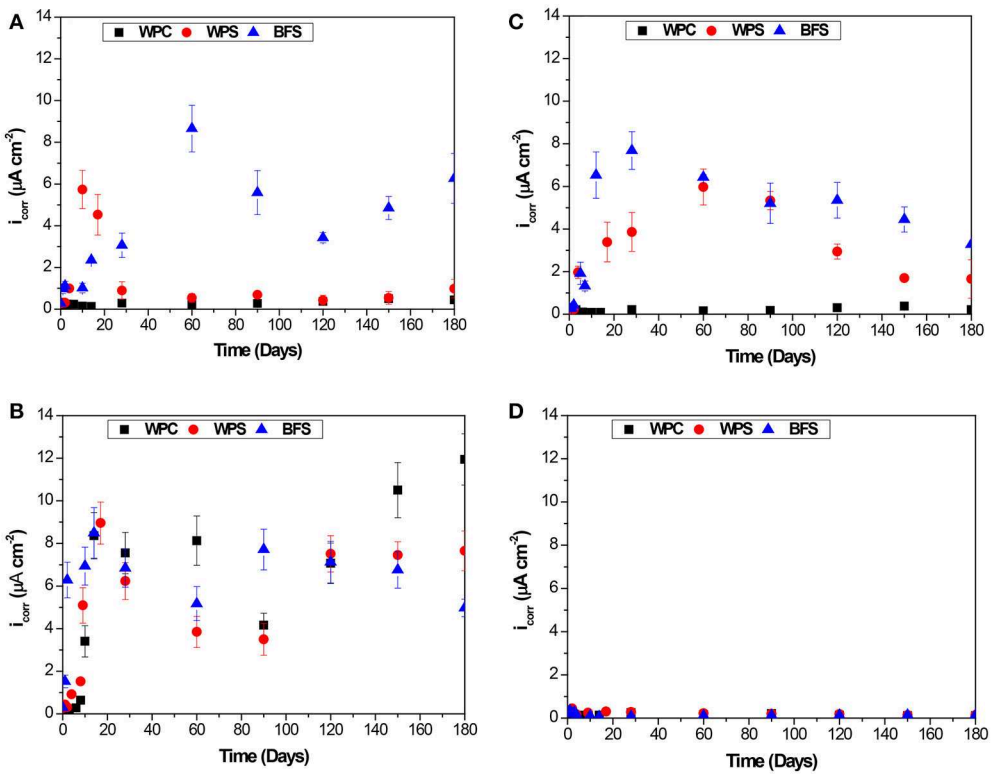


**FIGURE 6 |** Evolution of the corrosion current density values as a function of time, for steel embedded in BFS, WPS and WPC mortars immersed in **(A)** alkaline solution, **(B)** alkaline chloride-rich solution, **(C)** water, and **(D)** exposed to standard laboratory conditions, after 7 days of curing under sealed conditions.

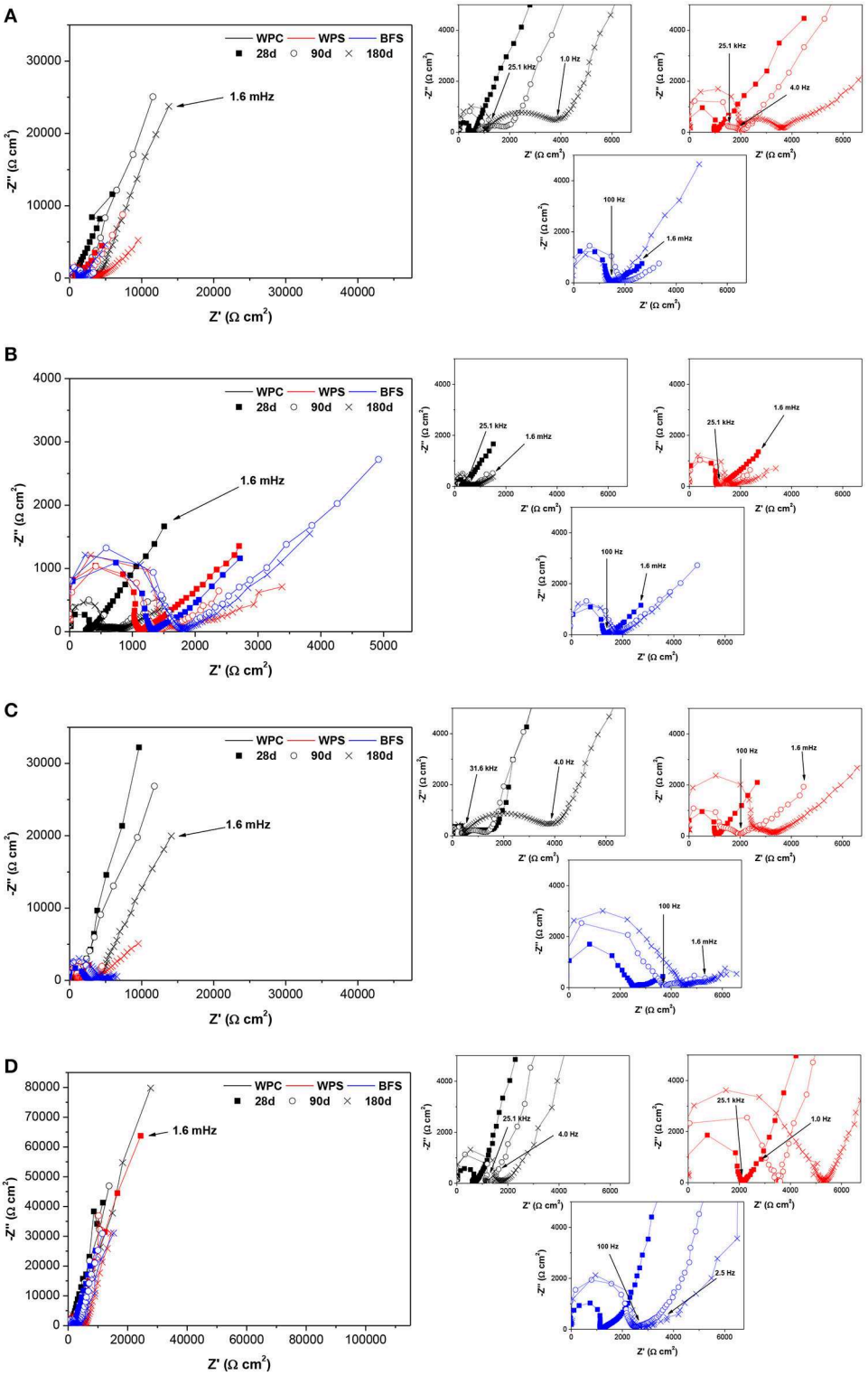


**FIGURE 7 |** Nyquist plots for BFS, WPS, and WPC mortars immersed in **(A)** alkaline solution, **(B)** alkaline chloride-rich solution, **(C)** water, and **(D)** exposed to standard laboratory conditions. In each part of the graphic, all data are shown overlaid for comparison in the left panel, and the smaller plots to the right show individually the time-dependence of the data obtained for each mortar type.

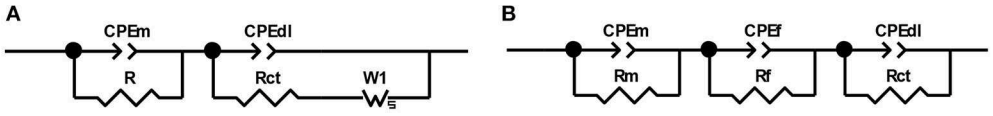


**FIGURE 8 |** Equivalent electrical circuits (EEC) used in fitting impedance spectra for BFS, WPS, and WPC mortars exposed to the four environments. **(A)** Samples with two time constants; **(B)** samples with three time constants.

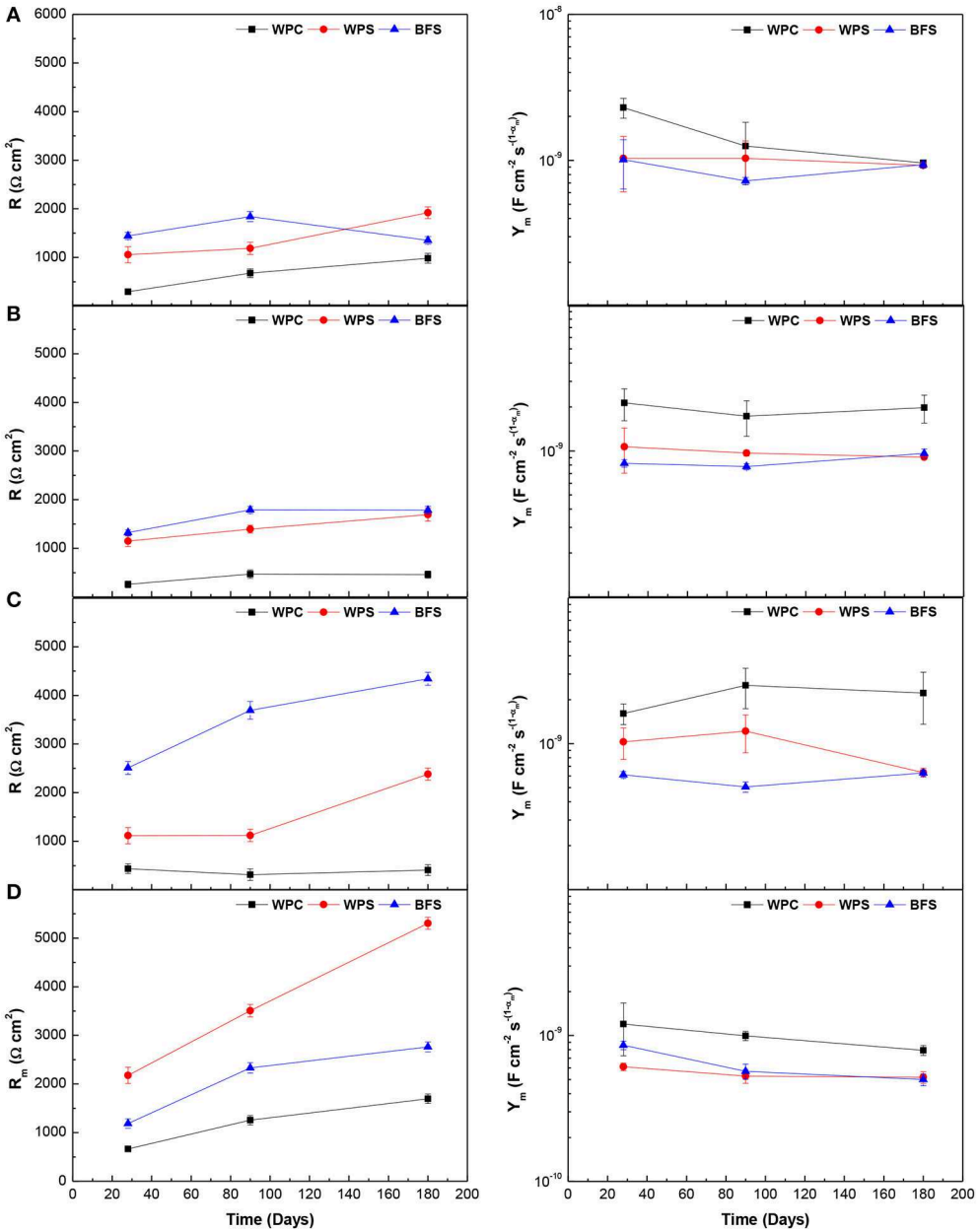


**FIGURE 9 |** Comparison of electrolyte and bulk matrix resistances $R$, and the mortar cover capacitance $Y_m$, for the three types of mortar exposed to: **(A)** alkaline solution, **(B)** alkaline chloride-rich solution, **(C)** water, and **(D)** standard laboratory conditions.

this simple electrochemical measurement from the actual corrosion of embedded steel. Therefore, the use of simple electrochemical criteria developed for plain Portland cement can generate misleading assumptions about the corrosion of embedded rebar in slag-containing mortars.

To provide further insight into the electrochemical behavior at the steel-mortar interface, electrical impedance spectroscopy was

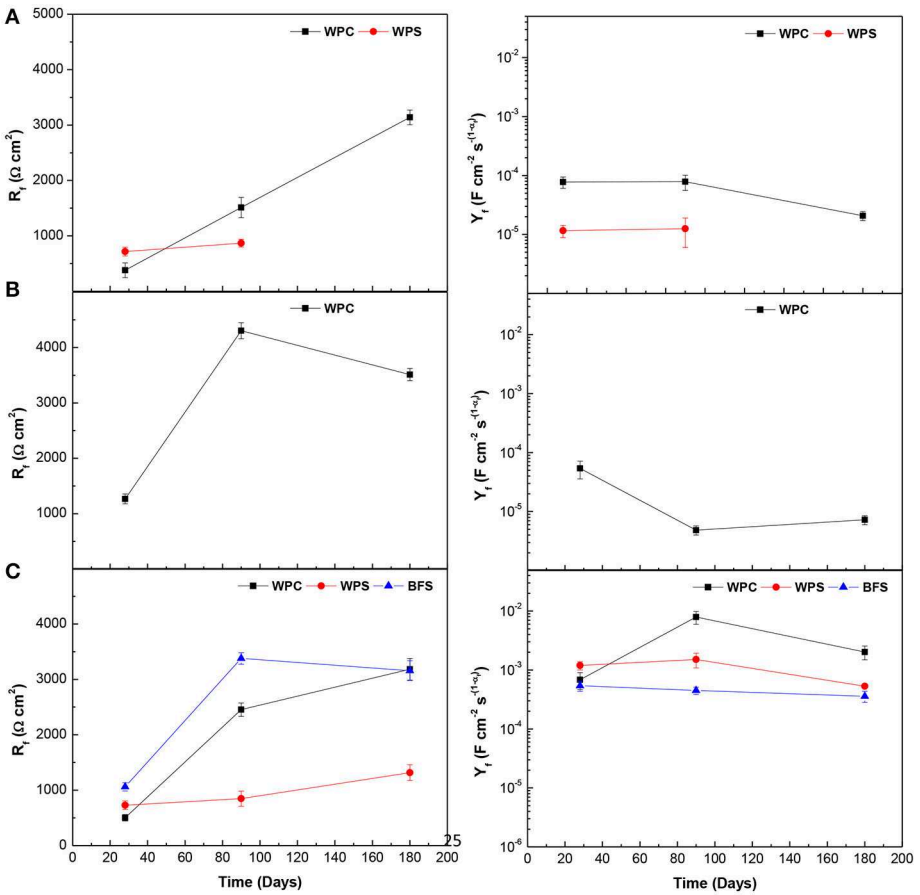


**FIGURE 10 |** Comparison of dielectric properties of rust layer/passive film layer resistance $R_f$, and capacitance $Y_f$, for the three types of specimens under different environments: **(A)** alkaline solution, **(B)** water, and **(C)** standard laboratory conditions.

conducted. **Figure 7** shows Nyquist plots recorded for the BFS, WPS, and WPC mortars after 180 days of exposure to each set of conditions. Some of the samples showed behavior that could be characterized by two distinct time constants: WPC mortars immersed in the alkaline chloride-rich solution, and BFS and WPS mortars in all immersion environments except for WPS in alkaline solution at early ages. The spectra obtained for all other specimens could only be appropriately described using three distinct time constants.

In the specimens which could be characterized by two time constants, the behavior in the high frequency range was related to the mortar cover properties (Castela et al., 2014), while the lower frequency range was associated with the steel/electrolyte interface (Tang et al., 2016). The impedance spectra of these specimens was fitted using the electrical equivalent circuit (EEC) shown in **Figure 8A**. The EEC is comprised of two parallel resistance ($R$) and constant phase element ($CPE$) combinations in series with each other. The first combination is constituted of $R$ and $CPE_m$, where the elements represent the electrolyte and bulk matrix resistances and the mortar cover capacitance, respectively. $R$ indicates the ability of the mortar to hinder the penetration of electrolytes with aggressive ions, and $CPE_m$ corresponds to the dielectric properties of the mortar. The second combination is constituted of $R_{ct}$ and $CPE_{dl}$, representing, respectively, the charge transfer resistance and the double layer capacitance at the electrolyte/steel interface.

A constant phase element ($CPE$) was used instead of a pure capacitator to describe the dielectric properties of material layers due to the inhomogeneities and discontinuities present (Bastidas, 2007). The impedance of a general $CPE$ with two parameters $Y$ and $\alpha$ can be expressed as: $Z_{CPE} = (Y)^{-1}(j\omega)^{-\alpha}$, where $Y$ is the $CPE$ constant with units of $\Omega^{-1}$ cm$^{-2}$ s$^{-(1-\alpha)}$, $\alpha$ is the $CPE$ exponent ($-1 < \alpha < 1$), $j$ is the imaginary unit ($j^2 = -1$), and $\omega$ is the angular frequency ($2\pi f$, where $f$ is the frequency).

Diffusional behavior was observed in these specimens, which may be attributed either to oxygen diffusion control due to the formation of the corrosion products (Tang et al., 2016), or to the diffusion of sulfide provided by the slag (Criado et al., 2018). Therefore, a diffusion Warburg ($W_1$) element was used to fit the

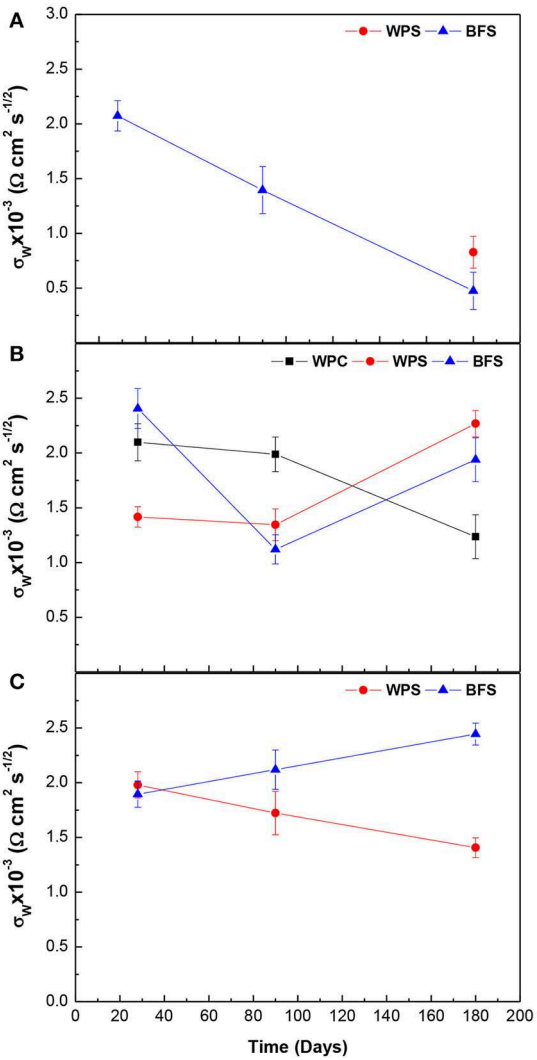


**FIGURE 11 |** Comparison of Warburg coefficient $\sigma_W$, for the three types of specimen under different environments: **(A)** alkaline solution, **(B)** alkaline chloride-rich solution, and **(C)** water.

impedance spectrum. The relationship between the $Y$ parameter and the Warburg coefficient ($\sigma_W$), is given by: $\sigma_W = \frac{1}{Y\sqrt{2}}$.

In the specimens with a third identifiable time constant, at high frequencies the Nyquist diagram showed a capacitive arc associated with the mortar cover properties, and the second time constant in the intermediate frequency regime was attributed to the passive film layer between the mortar cover and the steel (Sagoe-Crentsil et al., 1992; Ford et al., 1998). At low frequencies, the impedance response was again associated with the steel/electrolyte interface. For these specimens, the EEC shown in **Figure 8B** was employed, in which $R$ and $CPE_m$ represent the electrolyte and bulk matrix resistances and the mortar cover capacitance, respectively; $R_f$ and $CPE_f$ represent the dielectric properties of the passive film layer; and $R_{ct}$ and $CPE_{dl}$ represent the charge transfer resistance and double layer capacitance at the electrolyte/steel interface.

**Figure 9** displays the evolution of electrolyte and bulk matrix resistances ($R$) and the mortar cover capacitance [$CPE_m$ ($Y_m$)] as a function of time, for the three types of mortar under different environments. The electrolyte and bulk matrix resistances and the mortar cover capacitance reflect the ability of mortar to resist the penetration of electrolytes, and the dielectric properties of the mortar, respectively. Both parameters are directly related to the composition and pH of the pore solution, as well as the pore distribution and connectivity, which influence the measured conductivity and control the matrix permeability (Sagoe-Crentsil et al., 1992).

According to the data presented in **Figure 9**, BFS mortars presented the highest $R$-values and the lowest $Y_m$ values in all environments studied, except when the mortars were exposed to standard laboratory conditions. The microstructure of BFS is dominated by the relatively fast formation of calcium aluminosilicate hydrate (C-A-S-H) gel in the pore spaces at early age, while in Portland cement-containing binders a hydration layer has formed around the clinker grains, and the interstitial space fills only slowly (Gruskovnjak et al., 2006; Hubler et al., 2011). Therefore, BFS mortar had less capillary pore volume than WPC mortar, leading to a lower permeability, particularly at early age (7 days) and an increase of resistance took place. In slag blended cements, Ogirigbo et al. (Ogirigbo and Black, 2016) have reported that the replacement of clinker by slag resulted in a slight acceleration of the alite hydration. This can be attributed to the filler effect, where during the early stages of reaction, the limited reaction of slag grains allows more space for the formation of hydrates from the clinker hydration (Lothenbach et al., 2011; Berodier and Scrivener, 2014), leading to densification of the pore structure and a less electrically conductive microstructure in WPS mortars. Therefore, these had a higher resistivity than WPC mortars.

In general, $R$ or $R_m$ (bulk matrix resistance) tended to increase with time for the three types of mortar, likely due to the pore refinement by the mortar curing process. In addition, the resistance to chloride ingress increases over time, because the pores are blocked or reduced in width due to a gradually increasing degree of hydration, in particular due to hydration of slag in blended cements (Gaal et al., 2006), and correspondingly, the WPS mortars presented higher $R$ values than WPC mortars after 180 days of immersion in alkaline chloride-rich solution. The capacitance $Y_m$ of the mortar cover was constant or decreased slightly during the time of immersion, and these values were in the range of 1–50 nF cm$^{-2}$ s$^{-(1-\alpha_m)}$. This range was in reasonable agreement with other studies in the literature (Aperador et al., 2009; Sobhani and Najimi, 2013), although the numerical values cannot be directly compared due to differences in dimensionality as $\alpha_m$ varies.

The electrolyte and bulk matrix resistance values of BFS, WPS, and WPC mortars were quite similar when the specimens were immersed in the alkaline or alkaline chloride-rich solutions. However, these values increased when the specimens were immersed in water or exposed to standard laboratory conditions, particularly for BFS and WPS mortars. The water and the laboratory conditions were environments that presented fewer or no conductive species, respectively, leading to a higher resistivity

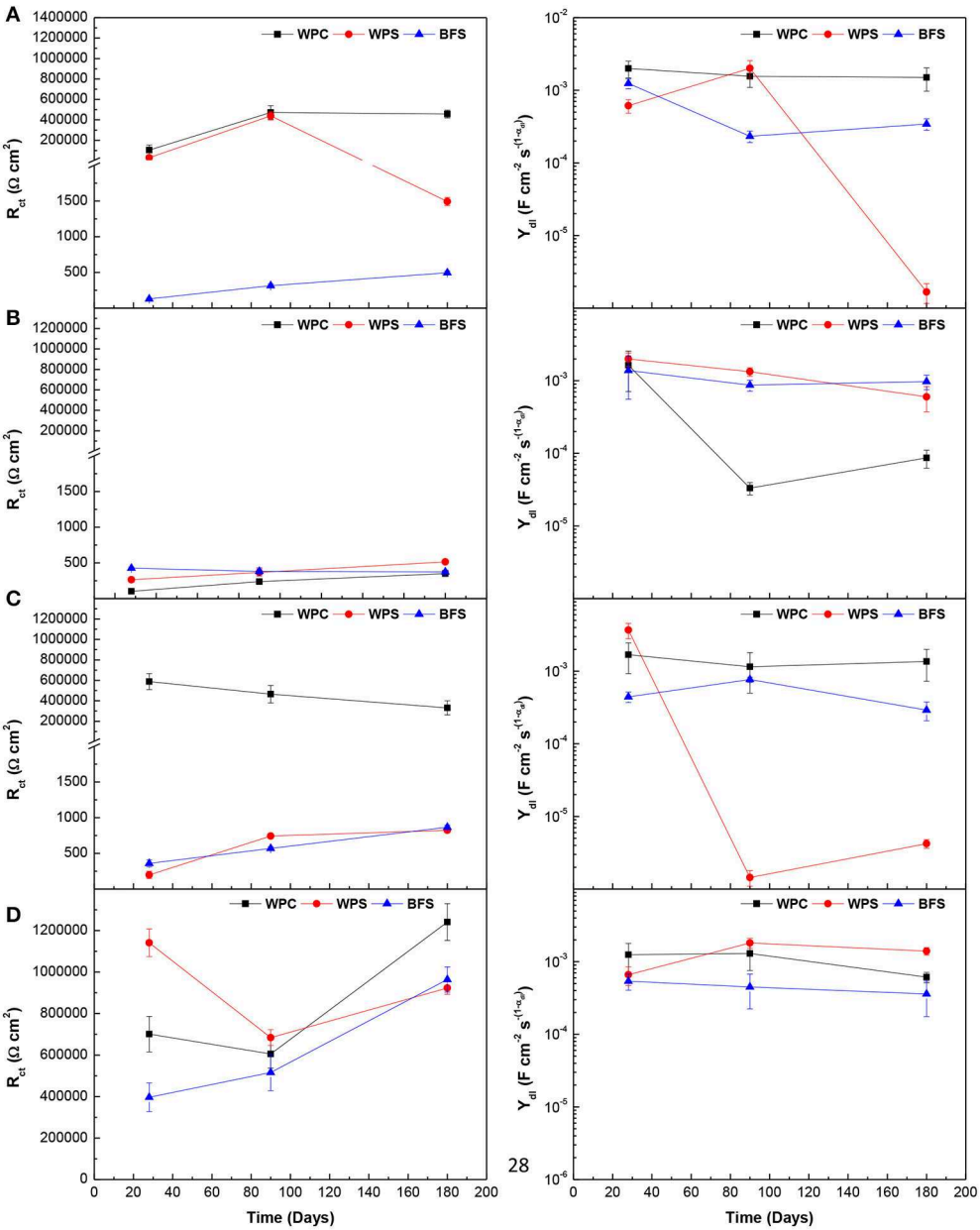


**FIGURE 12 |** Comparison of charge transfer resistance $R_{ct}$, and double layer capacitance $Y_{dl}$, for three types of specimens under different environments: **(A)** alkaline solution, **(B)** alkaline chloride-rich solution, **(C)** water, and **(D)** standard laboratory conditions.

of the mortars. The $Y_m$ values obtained when the three types of mortars were exposed to standard laboratory conditions were the smallest, indicating restriction of the movement of electrolytes through the mortar in the dry conditions as the pore fluid depercolated. In this latter environment, WPS mortars presented higher $R_m$ values than the other mortars.

**Figure 10** displays the evolution of resistance ($R_f$) and capacitance [$CPE_f(Y_f)$] of dielectric properties of passive film layer over time for three types of specimens immersed in the alkaline solution and the water, and exposed to standard laboratory conditions. The passive film layer resistance and capacitance measure the barrier performance of the passive film against the penetration of water and ions.

WPC seemed to be the matrix which favored the formation of a classical oxide passive layer in all environments studied, except in the alkaline chloride-rich solution, in which the passive layer was destabilized (as seen in **Figure 4**). For BFS and WPS mortars, the sulfide supplied by the slag was released and altered the passive film into a sulfidic layer that has a different electrochemical response (Mundra et al., 2017a). Therefore, the combination ($R_f$-$CPE_f$) was not observed, except when they were exposed to standard laboratory conditions or when WPS

mortar was immersed in the alkaline solution at early ages. In the case of BFS specimens exposed to air, the oxygen penetrated into the mortar and oxidized the sulfur species, while in the case of WPS, the reaction of slag was not the main initial hydration process and the release of sulfur ions did not take place at early age, as was observed through the open circuit potential. For standard laboratory conditions, BFS mortars presented the highest $R_f$ values and the lowest $Y_f$ values, indicating the passive layer had a high thickness and less porosity, and thus more resistance against the penetration of water and ions. This was consistent with the open circuit potential results where $E_{corr}$ values were always more positive than −0.152 V vs. Ag/AgCl, indicating that the steel was in a passive state. In general, the thickness and compactness of passive film layer increased with the time and an increase of $R_f$ and a decrease of $Y_f$ were observed, improving the protective properties of the layer.

The type of environment used to study of corrosion of the steel embedded in WPC mortars did not have a great influence in $R_f$ parameter. However, $Y_f$ values were clearly smaller when the mortars were immersed in the water. The passive film formed in these mortars presented high thickness and the steel remained in a passive state, as indicated by the corrosion potential and current density values presented above.

**Figure 11** shows the evolution of diffusion coefficient ($\sigma_w$) over time for the three types of specimens, under exposure to the alkaline and the alkaline chloride-rich solutions, and in water. The Warburg diffusion coefficient ($\sigma_w$) represents mass transport of species through the passive layer.

The $\sigma_w$ values are between 0.5 and 2.5 $\Omega$ cm$^2$ s$^{-1/2}$, independent of the nature of the mortar and the immersion time, and no clear trends were observed.

**Figure 12** displays the evolution of charge transfer resistance ($R_{ct}$) and double layer capacitance [$CPE_{dl}(Y_{dl})$] as a function of time for BFS, WPS and WPC mortars under the four exposure environments. Both parameters are related to the charge transfer and double layer characteristics at the interface between the steel and the electrolyte.

WPC mortars presented the highest charge transfer resistance values, more than $10^5$ $\Omega$ cm$^2$. These $R_{ct}$ values indicated the steel is a passive state (Andrade and Alonso, 1996) and the charge transfer controls the corrosion rate. BFS and WPS mortars usually presented very low $R_{ct}$ values, <1,500 $\Omega$ cm$^2$, except when WPS mortars were immersed in the alkaline solution at early ages and both mortars exposed to standard laboratory conditions. At early age, the sulfide has not yet been released to the pore solution, and when exposed in air, the sulfide ions have oxidized. These mortars with $R_{ct}$ < 1,500 $\Omega$ cm$^2$ also presented Warburg parameter $R_w$ (resistance to diffusion processes) values similar to the $R_{ct}$ values, suggesting a mixed charge transfer/diffusion control of the corrosion rate (Monticelli et al., 2016).

At 180 days, the charge transfer resistance values of WPC mortars immersed in the alkaline solution and in water, and of the three mortars exposed to standard laboratory conditions, were similar or larger than those at 30 days, indicating that the steel remained in a passive state over the entire duration of testing. In the alkaline solution and the water, the steel was in a passive state, but depending on the type of mortar, $R_{ct}$ values were in the range $10^5 - 6 \times 10^5$ $\Omega$ cm$^2$ for WPC mortar, and 130–1,500 $\Omega$ cm$^2$ for WPS and BFS mortars. This difference in $R_{ct}$ values was due to the presence of sulfide which diffused through the pore solution to the surface of the steel, favoring the diffusion processes over those of charge transfer at the steel/electrolyte interface. In the alkaline chloride-rich solution, the $R_{ct}$ values vary between 100 and 515 $\Omega$ cm$^2$ for the three types of mortar. These small values were due to the breakdown of the passive film in the presence of chloride ions in the case of WPC mortars. In the other two mortars, transport of ions took place due to the presence of sulfide in the pore solution, which implied a reduction of $R_{ct}$ values. In standard laboratory conditions, $R_{ct}$ values are in the range $6 \times 10^5 - 2 \times 10^6$ $\Omega$ cm$^2$, confirming the passivation of steel (Andrade and Alonso, 1996).

The double layer capacitance for all samples was in the range $3.6 \times 10^{-3}$–$1.4 \times 10^{-4}$ F cm$^{-2}$ s$^{-(1-\alpha_{dl})}$; this parameter was not evidently influenced by the chemical composition of the mortars, the immersion time and the exposure environments, showing no clear trends. However, this range is in reasonable agreement with other studies of AAMs (Aperador et al., 2009; Criado et al., 2012; Monticelli et al., 2016).

## CONCLUSIONS

In this study, mortars with slag contents ranging from 100 to 0% were immersed in different environments, and the evolution of electrochemical parameters as a function of time was determined. The current density values measured for the alkali-activated slag mortars and the blended WPC-slag mortars immersed in alkaline solution and in water were high, which would usually be taken to indicate high or very high risk of corrosion, but extracted rebars did not show evident pits or corrosion product layers. Therefore, these high current densities indicate that the current is flowing due to the oxidation of the sulfide supplied by the slag, and are not necessarily an indication of a corrosion process. In the presence of high concentrations of sufide around the steel surface, the development of a hydrated iron oxide passivating film is hindered and a steel surface rich in various Fe-S species is favored. It is also clear that there is a need to further examine the Tafel constants conventionally used for Portland cement-based binders, to determine whether they are valid for slag-rich and/or alkali-activated cements.

When mortars were immersed in an alkaline chloride-rich solution, very negative corrosion potentials and high current density values were obtained for both BFS and WPC mortars, indicating a lower resistance to chloride-induced corrosion of steel, but the observation of extracted rebars showed that the steel embedded in BFS mortars did not show any evidence of corrosion. The presence of sulfide supplied by the slag affected strongly the electrochemical measurements. Based on the results

of this study, differences in the mechanisms of passivation and corrosion existed between steel embedded in alkali-activated slag mortars and that in white Portland mortars in the presence of chloride ions, where a higher resistance to chloride-induced corrosion of steel was provided by BFS mortars.

## AUTHOR CONTRIBUTIONS

MC and JP designed the experimental plan. MC conducted experimental and modeling work and data analysis. MC and JP jointly interpreted the data and drafted the paper.

## ACKNOWLEDGMENTS

The research leading to these results received funding from the European Research Council under the European Union's Seventh Framework Programme (FP/2007-2013)/ERC Grant Agreement #335928. The authors would like to acknowledge the technical support provided by Dr. Oday Hussein. The authors would also like to thank Mr. Kieran Nash at The University of Sheffield for supplying the rebars. This research was performed in part at the MIDAS Facility, at The University of Sheffield, which was established with support from the Department of Energy and Climate Change.

## REFERENCES

Andrade, C., and Alonso, C. (1996). Corrosion rate monitoring in the laboratory and on-site. *Construct. Build. Mater.* 10, 315–328.

Andrade, C., Castelo, V., Alonso, C., and Gonzalez, J. A. (1986). "The determination of the corrosion rate of steel embedded in concrete by the polarization resistance and AC impedance methods," in *ASTM STP 906, Corrosion Effect of Stray Currents and the Techniques for Evaluating Corrosion of Rebars in Concrete,* ed V. Chaker (West Conshohocken, PA: ASTM International), 43–63.

Aperador, W., Mejía de Gutierrez, R., and Bastidas, D. M. (2009). Steel corrosion behaviour in carbonated alkali-activated slag concrete. *Corros. Sci.* 51, 2027–2033. doi: 10.1016/j.corsci.2009.05.033

ASTM International (2015). *ASTM C876-15, Standard Test Method for Corrosion Potentials of Uncoated Reinforcing Steel in Concrete*. West Conshohocken, PA: ASTM International.

Babaee, M., and Castel, A. (2016). Chloride-induced corrosion of reinforcement in low-calcium fly ash-based geopolymer concrete. *Cement Con. Res.* 88, 96–107. doi: 10.1016/j.cemconres.2016.05.012

Bastidas, D. M. (2007). Interpretation of impedance data for porous electrodes and diffusion processes. *Corrosion* 63, 515–521. doi: 10.5006/1.3278402

Berodier, E., and Scrivener, K. (2014). Understanding the filler effect on the nucleation and growth of C-S-H. *J. Am. Ceram. Soc.* 97, 3764–3773. doi: 10.1111/jace.13177

Bertolini, L., Elsener, B., Pedeferri, P., Redaelli, E., and Polder, R. B. (2013). *Corrosion of Steel in Concrete: Prevention, Diagnosis, Repair*. Oxford, UK: John Wiley & Sons.

Böhni, H. (2005). *Corrosion in Reinforced Concrete Structures*. Abington; Cambridge, England: Woodhead Publishing Ltd.

British Standards Institute (2016). *BS 4449:2005+A3:2016: Steel for the Reinforcement of Concrete. Weldable Reinforcing Steel. Bar, Coil and Decoiled Product. Specification*. London: BSI Publications.

Castela, A. S., da Fonseca, B. S., Duarte, R. G., Neves, R., and Montemor, M. F. (2014). Influence of unsupported concrete media in corrosion assessment for steel reinforcing concrete by electrochemical impedance spectroscopy. *Electrochim. Acta* 124, 52–60. doi: 10.1016/j.electacta.2013.11.157

Cheng, A., Huang, R., Wu, J.-K., and Chen, C.-H. (2005). Influence of GGBS on durability and corrosion behavior of reinforced concrete. *Mater. Chem. Phys. 93*, 404–411. doi: 10.1016/j.matchemphys.2005.03.043

Criado, M., Bernal, S. A., Garcia-Triñanes, P., and Provis, J. L. (2018). Influence of slag composition on the stability of steel in alkali-activated cementitious materials. *J.Mat. Sci.* 53, 5016–5035. doi: 10.1007/s10853-017-1919-3

Criado, M., Monticelli, C., Fajardo, S., Gelli, D., Grassi, V., and Bastidas, J. M. (2012). Organic corrosion inhibitor mixtures for reinforcing steel embedded in carbonated alkali-activated fly ash mortar. *Construct. Build. Mater.* 35, 30–37. doi: 10.1016/j.conbuildmat.2012.02.078

de la Fuente, D., Alcántara, J., Chico, B., Díaz, I., Jiménez, J. A., and Morcillo, M. (2016). Characterisation of rust surfaces formed on mild steel exposed to marine atmospheres using XRD and SEM/Micro-raman techniques. *Corros. Sci.* 110, 253–264. doi: 10.1016/j.corsci.2016.04.034

European Committee for Standardization (2005). *Methods of Testing Cement - Part 1: Determination of Strength (EN 196-1)*. Brussels.

European Committee for Standardization (2011). *EN 197-1:2011, Cement. Part 1: Composition, Specifications and Conformity Criteria for Common Cements*. Brussels.

Ford, S. J., Shane, J. D., and Mason, T. O. (1998). Assignment of features in impedance spectra of the cement-paste/steel system. *Cement Conc. Res.* 28, 1737–1751.

Gaal, G. C., Koenders, E. A., and Polder, R. B. (2006). "Ageing effect of chloride diffusion coefficient," in *ConcreteLife'06, International RILEM-JCI Seminar on Concrete Durability and Service Life Planning: Curing, Crack Control, Performance in Harsh Environments* (Delft: RILEM Publications SARL).

Garcia, V., François, R., Carcasses, M., and Gegout, P. (2014). Potential measurement to determine the chloride threshold concentration that initiates corrosion of reinforcing steel bar in slag concretes. *Mater. Struct.* 47, 1483–1499. doi: 10.1617/s11527-013-0130-5

Ghantous, R. M., Poyet, S., L'Hostis, V., Tran, N.-C., and François, R. (2017). Effect of crack openings on carbonation-induced corrosion. *Cement Conc. Res.* 95, 257–269. doi: 10.1016/j.cemconres.2017.02.014

Glasser, F. (2001). Mineralogical aspects of cement in radioactive waste disposal. *Mineral. Mag.* 65, 621–633. doi: 10.1180/0026461013170 18442

Glasser, F. P. (1991). "Chemical, mineralogical, and microstructural changes occurring in hydrated slag-cement blends," in *Materials Science of Concrete II,* eds J. Skalny and S. Mindess (Westerville, OH: American Ceramic Society), 41–81.

Gruskovnjak, A., Lothenbach, B., Holzer, L., Figi, R., and Winnefeld, F. (2006). Hydration of alkali-activated slag: comparison with ordinary Portland cement. *Adv. Cement Res.* 18, 119–128. doi: 10.1680/adcr.2006.18.3.119

Gu, P., Beaudoin, J., Zhang, M.-H., and Malhotra, V. (2000). Performance of reinforcing steel in concrete containing silica fume and blast-furnace slag ponded with sodium-chloride solution. *ACI Mater. J.* 97, 254–262. doi: 10.14359/4620

Holloway, M., and Sykes, J. M. (2005). Studies of the corrosion of mild steel in alkali-activated slag cement mortars with sodium chloride admixtures by a galvanostatic pulse method. *Corros. Sci.* 47, 3097–3110. doi: 10.1016/j.corsci.2005.05.035

Huang, R., Chang, J.-J., and Wu, J.-K. (1996). Correlation between corrosion potential and polarization resistance of rebar in concrete. *Mater. Lett.* 28, 445–450.

Hubler, M. H., Thomas, J. J., and Jennings, H. M. (2011). Influence of nucleation seeding on the hydration kinetics and compressive strength of alkali activated slag paste. *Cement Conc. Res.* 41, 842–846. doi: 10.1016/j.cemconres.2011.04.002

Ke, X., Bernal, S. A., Hussein, O. H., and Provis, J. L. (2017a). Chloride binding and mobility in sodium carbonate-activated slag pastes and mortars. *Mater. Struct.* 50:252. doi: 10.1617/s11527-017-1121-8

Ke, X., Bernal, S. A., and Provis, J. L. (2017b). Uptake of chloride and carbonate by Mg-Al and Ca-Al layered double hydroxides in simulated pore solutions of alkali-activated slag cement. *Cement Conc. Res.* 100, 1–13. doi: 10.1016/j.cemconres.2017.05.015

Larroumet, D., Greenfield, D., Akid, R., and Yarwood, J. (2007). Raman spectroscopic studies of the corrosion of model iron electrodes in sodium chloride solution. *J. Raman Spectrosc.* 38, 1577–1585. doi: 10.1002/jrs.1810

L'Hostis, V., Amblard, E., Guillot, W., Paris, C., and Bellot-Gurlet, L. (2013). Characterisation of the steel concrete interface submitted to chloride-induced-corrosion. *Mater. Corros.* 64, 185–194. doi: 10.1002/maco.201106488

Lloyd, R. R., Provis, J. L., and van Deventer, J. S. J. (2010). Pore solution composition and alkali diffusion in inorganic polymer cement. *Cement Conc. Res.* 40, 1386–1392. doi: 10.1016/j.cemconres.2010.04.008

Lothenbach, B., Scrivener, K., and Hooton, R. D. (2011). Supplementary cementitious materials. *Cement Conc. Res.* 41, 1244–1256. doi: 10.1016/j.cemconres.2010.12.001

Ma, Q., Nanukuttan, S. V., Basheer, P. A. M., Bai, Y., and Yang, C. (2016). Chloride transport and the resulting corrosion of steel bars in alkali activated slag concretes. *Mater. Struct.* 49, 3663–3677. doi: 10.1617/s11527-015-0747-7

Misawa, T., Asami, K., Hashimoto, K., and Shimodaira, S. (1974). The mechanism of atmospheric rusting and the protective amorphous rust on low alloy steel. *Corros. Sci.* 14, 279–289.

Monticelli, C., Natali, M. E., Balbo, A., Chiavari, C., Zanotto, F., Manzi, S., et al. (2016). A study on the corrosion of reinforcing bars in alkali-activated fly ash mortars under wet and dry exposures to chloride solutions. *Cement Conc. Res.* 87, 53–63. doi: 10.1016/j.cemconres.2016.05.010

Mundra, S., Bernal, S. A., Criado, M., Hlaváček, P., Ebell, G., Reinemann, S., et al. (2017a). Steel corrosion in reinforced alkali-activated materials. *RILEM Tech. Lett.* 2, 33–39. doi: 10.21809/rilemtechlett.2017.39

Mundra, S., Bernal, S. A., and Provis, J. L. (2017b). "Corrosion initiation of steel reinforcement in simulated alkali-activated slag pore solution," in *1st International Conference of Construction Materials for Sustainable Future, CoMS2017* (Zadar).

Mundra, S., Bernal, S. A., and Provis, J. L. (2017c). "Durability of steel reinforced alkali-activated concretes in the presence of chloride," in *The Future of Cement, 200 Years after Louis Vicat* (Paris).

Mundra, S., Criado, M., Bernal, S. A., and Provis, J. L. (2017d). Chloride-induced corrosion of steel rebars in simulated pore solutions of alkali-activated concretes. *Cement Conc. Res.* 100, 385–397. doi: 10.1016/j.cemconres.2017.08.006

Neff, D., Bellot-Gurlet, L., Dillmann, P., Reguer, S., and Legrand, L. (2006). Raman imaging of ancient rust scales on archaeological iron artefacts for long-term atmospheric corrosion mechanisms study. *J. Raman Spectrosc.* 37, 1228–1237. doi: 10.1002/jrs.1581

Ogirigbo, O. R., and Black, L. (2016). Influence of slag composition and temperature on the hydration and microstructure of slag blended cements. *Construct. Build. Mater.* 126, 496–507. doi: 10.1016/j.conbuildmat.2016.09.057

Park, J. W., Ann, K. Y., and Cho, C.-G. (2015). Resistance of alkali-activated slag concrete to chloride-induced corrosion. *Adv. Mater. Sci. Eng.* 2015:273101. doi: 10.1155/2015/273101

Sagoe-Crentsil, K. K., Glasser, F. P., and Irvine, J. T. S. (1992). Electrochemical characteristics of reinforced concrete corrosion as determined by impedance spectroscopy. *Br. Corros. J.* 27, 113–118.

Sobhani, J., and Najimi, M. (2013). Electrochemical impedance behavior and transport properties of silica fume contained concrete. *Construct. Build. Mater.* 47, 910–918. doi: 10.1016/j.conbuildmat.2013.05.010

Song, H.-W., and Saraswathy, V. (2006). Studies on the corrosion resistance of reinforced steel in concrete with ground granulated blast-furnace slag - an overview. *J. Hazard. Mater.* 138, 226–233. doi: 10.1016/j.jhazmat.2006.07.022

Stern, M., and Geary, A. L. (1957). Electrochemical polarization I. A theoretical analysis of the shape of polarization curves. *J. Electrochem. Soc.* 104, 56–63.

Tang, F., Chen, G., and Brow, R. K. (2016). Chloride-induced corrosion mechanism and rate of enamel- and epoxy-coated deformed steel bars embedded in mortar. *Cement Conc. Res.* 82, 58–73. doi: 10.1016/j.cemconres.2015.12.015

Topçu, I. B., and Boga, A. R. (2010). Effect of ground granulate blast-furnace slag on corrosion performance of steel embedded in concrete. *Mater. Des.* 31, 3358–3365. doi: 10.1016/j.matdes.2010.01.057

Torres Gomez, R., Aperador, W., Vera, E., Mejía de Gutiérrez, R., and Ortiz, C. (2010). Study of steel corrosion embedded in AAS concrete under chlorides. *Dyna* 77, 52–59. Available online at: http://www.scielo.org.co/scielo.php?script=sci_arttext&pid=S0012-73532010000400006

Tromans, D. (1980). Anodic polarization behavior of mild steel in hot alkaline sulfide solutions. *J. Electrochem. Soc.* 127, 1253–1256.

Wan, M., Schröder, C., and Peiffer, S. (2017). Fe(III):S(-II) concentration ratio controls the pathway and the kinetics of pyrite formation during sulfidation of ferric hydroxides. *Geochim. Cosmochim. Acta* 217, 334–348. doi: 10.1016/j.gca.2017.08.036

Yeau, K. Y., and Kim, E. K. (2005). An experimental study on corrosion resistance of concrete with ground granulate blast-furnace slag. *Cement Conc. Res.* 35, 1391–1399. doi: 10.1016/j.cemconres.2004.11.010

**Conflict of Interest Statement:** The authors declare that the research was conducted in the absence of any commercial or financial relationships that could be construed as a potential conflict of interest.